Supporting Information

Rapid, Sensitive, Label-free Electrical Detection of SARS-CoV-2 in Nasal Swab Samples

Hyun-June Jang[1,2], Wen Zhuang[1,2], Xiaoyu Sui[1,2], Byunghoon Ryu[2], Xiaodan Huang[1], Min Chen[1], Xiaolei Cai[1], Haihui Pu[1,2], Kathleen Beavis[3], Jun Huang[1], Junhong Chen[1,2*]

[1]Pritzker School of Molecular Engineering, University of Chicago, Chicago, IL 60637, USA

[2]Chemical Sciences and Engineering Division, Physical Sciences and Engineering Directorate, Argonne National Laboratory, Lemont, IL 60439, USA

[3]Department of Pathology, University of Chicago, Chicago, IL 60637, USA

*Correspondence: junhongchen@uchicago.edu

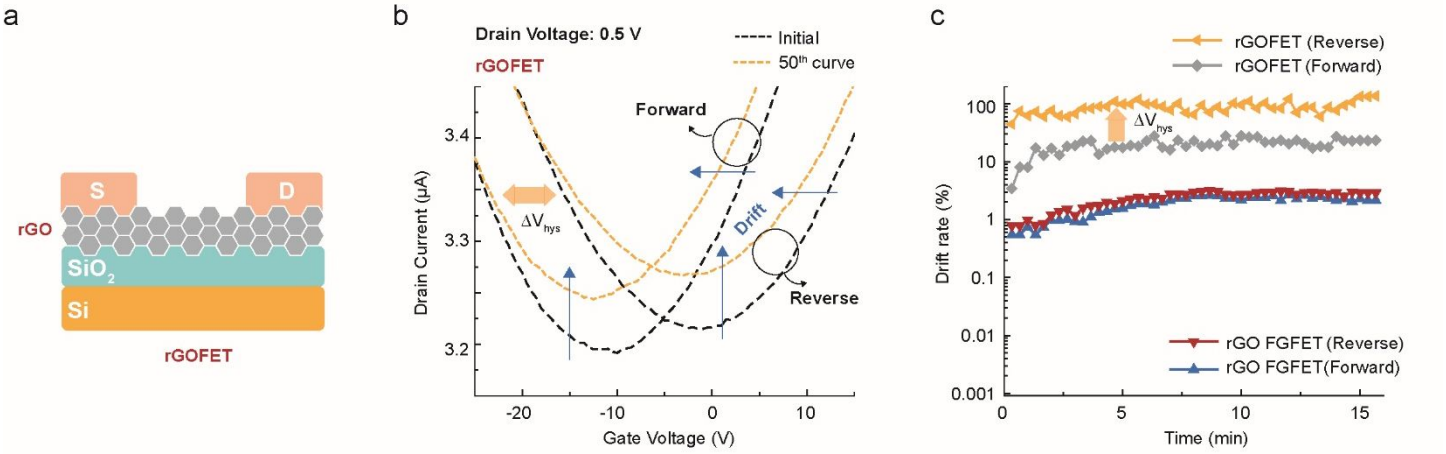

Figure S1. (a) Schematic images of conventional rGOFET structure with bottom gate; rGO identically processed to that of RFG was used as a semiconducting layer for this case. (b) Transfer characteristics of rGOFET measured for 50 gate voltage cycles in a double sweeping mode via the bottom gate without any solution environment on the rGO layer. Huge hysteresis and drift components are shown from rGO channels between initial and final transfer curves. (c) Drift rate of rGO RFGFET and rGOFET measured for 50 gate voltage cycles in a double sweeping mode. Insignificant drifts were shown from rGO RFG even in contact with a PBS solution (0.7%) despite possible interactions between ions in PBS and numerous defects and interface trap densities present between rGO and SiO_2 substrate. This is because influences of those interactions are incapacitated by blocking any chance of current flows into 2D rGO layer, which is a source of energy for interactions, due to the high input impedance of FET and the insulator in the RFG structure. rGOFET without solution environment on the rGO layer has at least 50 times larger drift with significant hysteresis for a double sweeping mode due to numerous defects and interface trap densities residing in rGO.

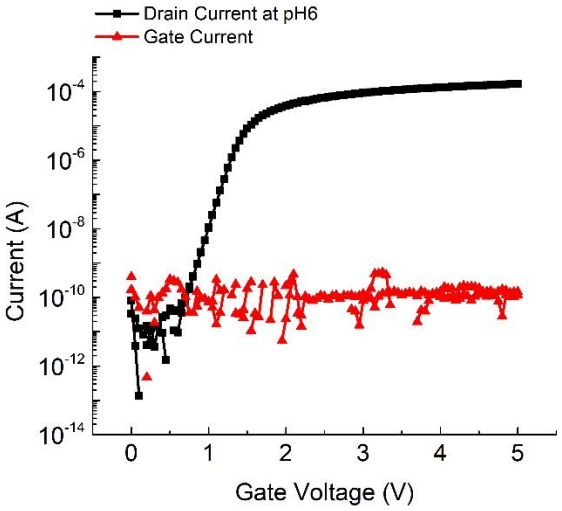

Figure S2. A transfer curve of the RFGFET with an rGO sensing membarne on the RFG measured in a pH6 buffer solution. Drain voltage sets at 50 mV. An Ag/AgCl reference electrode contacted the pH6 solution on the RFG to apply the gate volatge in a range from 0 to 5V. During operation of RFGFET, picoampere levels of gate leakage currents are shown, indicating that there is mostly no current flow through rGO sensing membrane on the FG due to a high gate input impedence given by SiO_2 insulating layer of the RFG and a gate insulator of commerical FET.

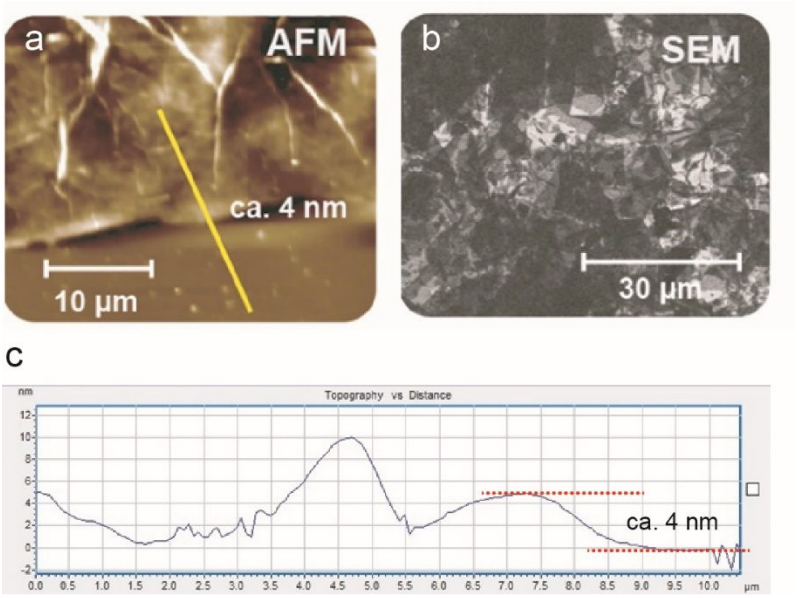

Figure S3. (a) Topographic image of 2D multilayers rGO measured by atomic force microscopy (AFM). (b) Scanning electron micoscopy (SEM) image of 2D multilayers rGO covering SiO_2 surface on the RFG. (c) Height profile of 2D multilayers rGO in Figure S3a.

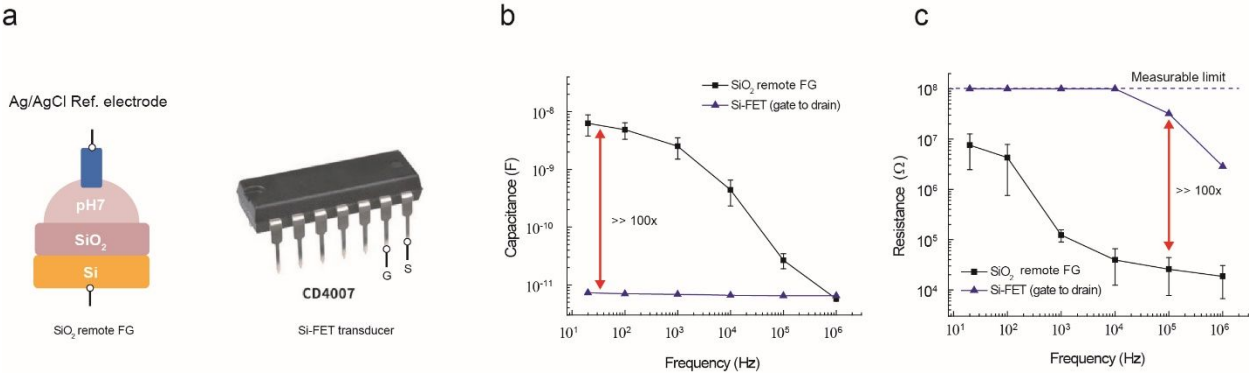

Figure S4. (a) Schematic images of device structure for impedance measurement of RFG and commercial FET (CD4007, n-type). Frequency vs (b) capacitance and (c) resistance of a 300-nm-thick SiO_2 and gate-drain of MOSFET chip. For measurement of remote RFG, 50 μl pH7 solution was added on the top of SiO_2 surface. AC frequency was applied from the Ag/AgCl reference electrode to the bottom silicon electrode of each RFG. To measure impedance of the MOSFET chip, AC frequency was applied from the gate to source terminal. The level of voltage was set at 1 V during capacitance and resistance measurements. The input impedance of MOSFET is much higher than those of SiO_2 RFG, suggesting that the effect of impedance of RFGs on total impedance of RFGFET is insignificant.

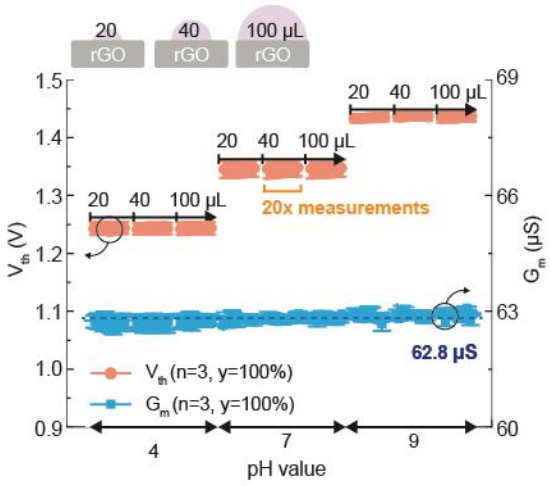

Figure S5. V_{th} and G_m levels of rGO RFGFET measured in pH4, pH7, and pH10 buffer solutions with different volumes of each solution on rGO surface of the RFG. V_{th} is only changed by responding to the pH value, not by contact areas of buffer solution. It is noted that G_m is independent variables from any volume size of solution and changes in surface potentials.

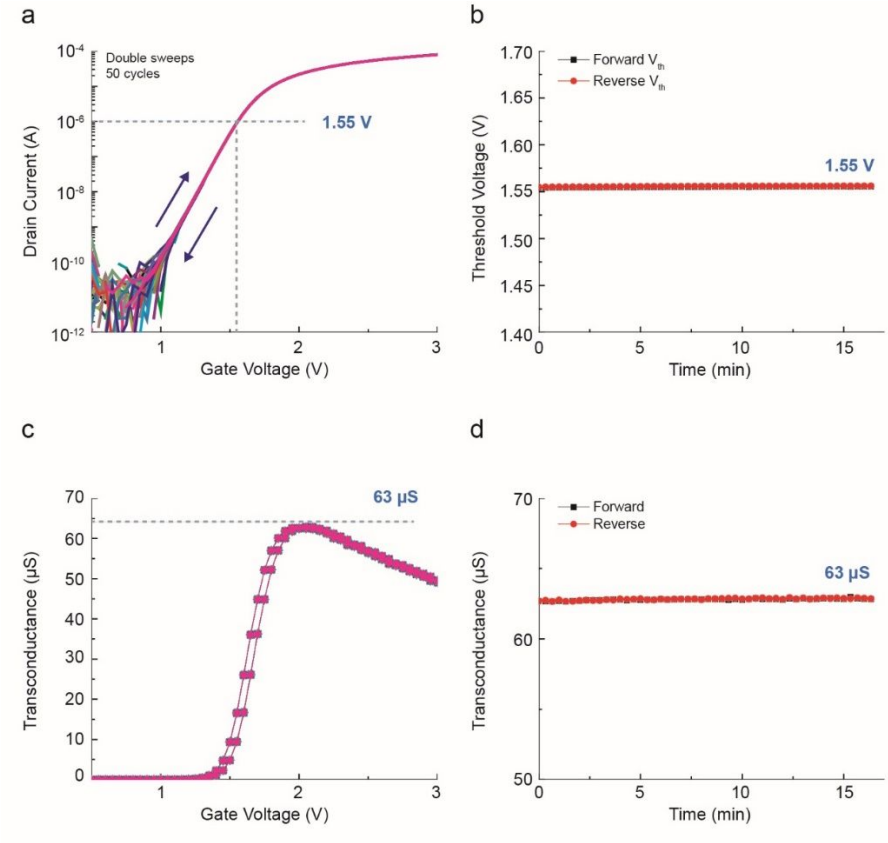

Figure S6. (a) Transfer curves of a metal-oxide-semiconductor field-effect transistor (MOSFET), without connecting the RFG, measured by a double-sweeping mode for 50 gate voltage cycles in a range from 0 to 5 V; drain voltage set at 50 mV over the measurements. (b) V_{th} of the MOSFET measured by each forward- and reverse-sweeping mode over time; no drift and hysteresis in V_{th} (1. 55 V) shown over time. (c) Transconductance (G_m) curves of the MOSFET measured at Figure S6a. (d) G_m of the MOSFET measured by each forward- and reverse-sweeping mode over time; no drift and hysteresis in G_m (63 μS) shown over time.

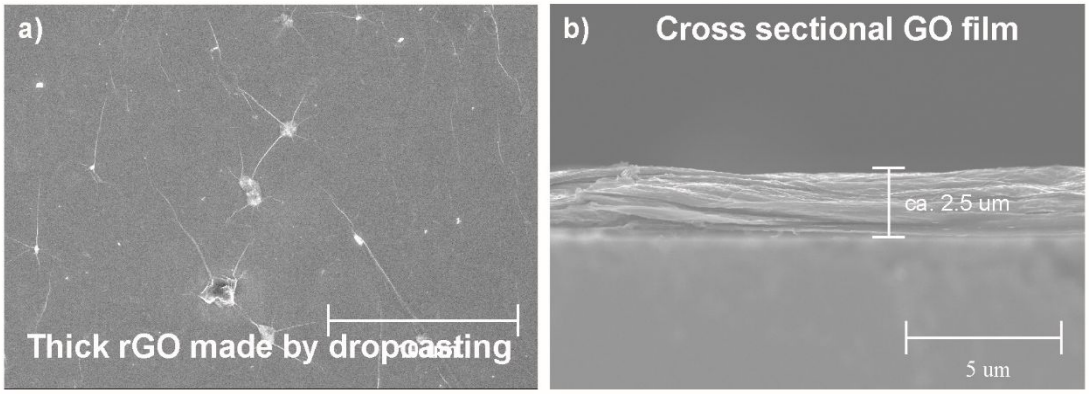

Figure S7. SEM images of a continuous thick GO film. (b) Cross-sectional SEM image of thick GO film made by drop-casting method. The thickness of the GO film was measured to be about 2.5 μm from cross-sectional SEM images of the GO film.

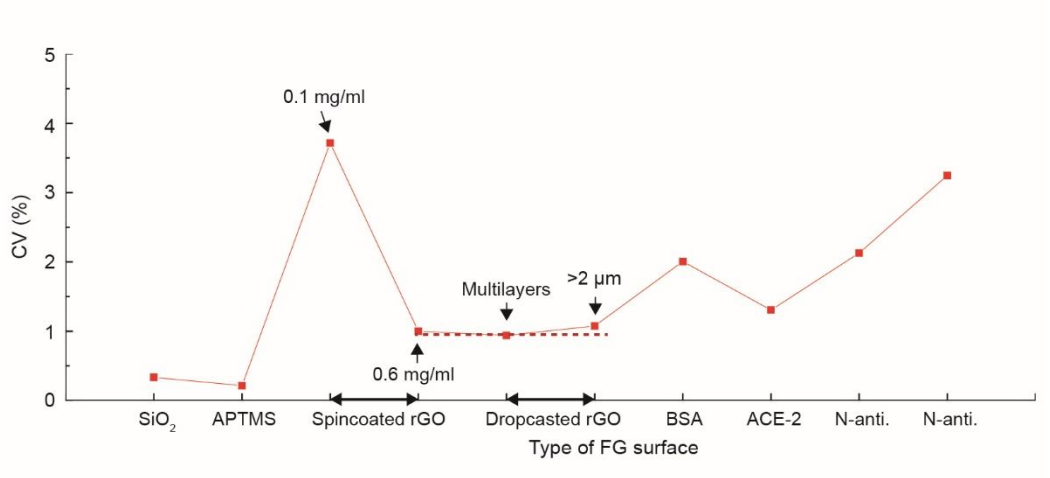

Figure S8. CV values calculated from raw data of V_{th} for each RFG condition in Figure 1c. CV is less than 4% over all conditions.

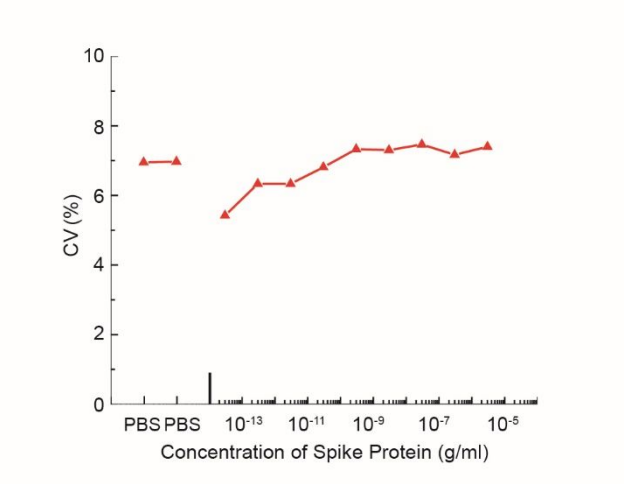

Figure S9. CV values calculated from raw data of V_{th} for each concentration of spike protein over 6 devices in Figure 2b. CV is less than 8% over all measurements.

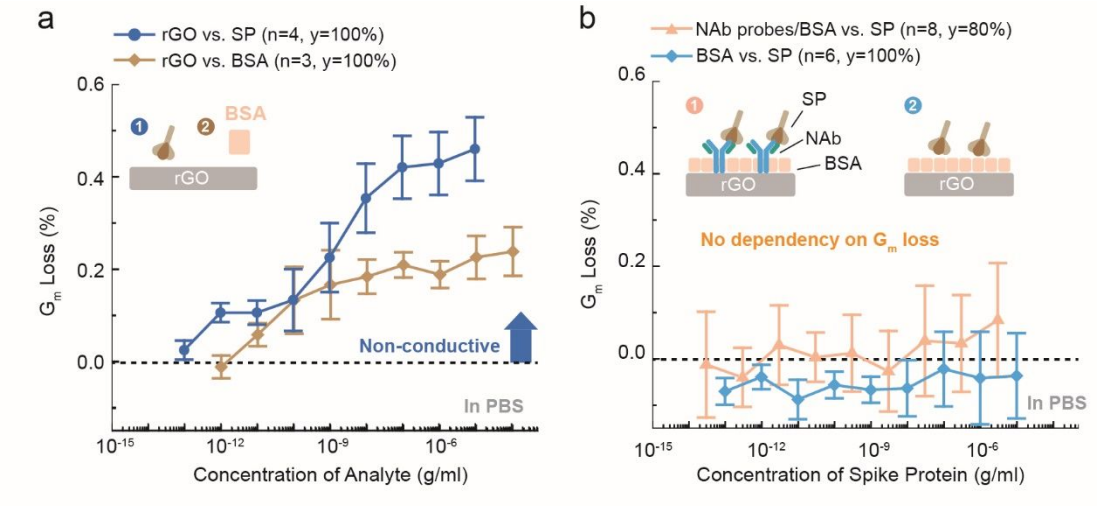

Figure S10. (a) G_m loss of pristine rGO vs. concentrations of SP and BSA, respectively. G_m loss is calculated as $(G_{FET} – G_m)/G_{FET}$ where G_{FET} is defined as G_m of the MOSFET (63 μS). (b) G_m loss of NAb-funcitonalized rGO and BSA-blocked rGO (no probe) vs. concentrations of SP, respectively.

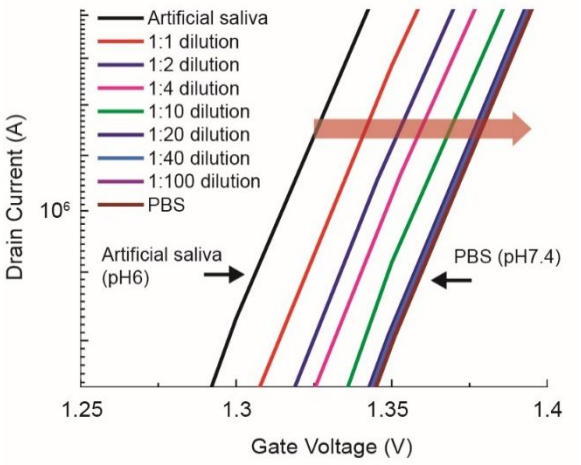

Figure S11. Transfer curves of a bare rGO surface measured in a pure artificial saliva, artificial saliva mixtures with different dilution ratios between artificial saliva and 0.05 × PBS, and a pure 0.05 × PBS. A pure artificial saliva at pH 6 was diluted in a 0.05 × PBS solution at pH 7.4 with a different ratio of the PBS solution. Transfer curve of the artificial solution mixture diluted in a ratio of 1:20 (artificial saliva:PBS) is mostly overlapping with that of a pure 0.05 × PBS, implying that the pH value of both the artificial solution mixture and the 0.05 × PBS was controlled at 7.4.

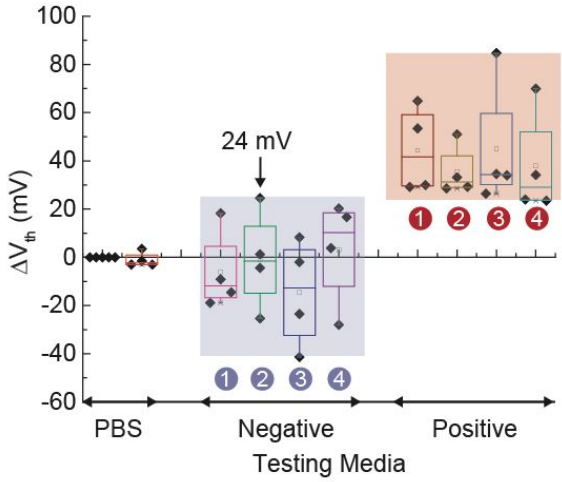

Figure S12. ΔV_{th} distributions of raw data from clinical sample tests in Figure 3b. Maximum ΔV_{th} of samples tested negative is 24 mV, which is defined as a maximum background noise level of this system.

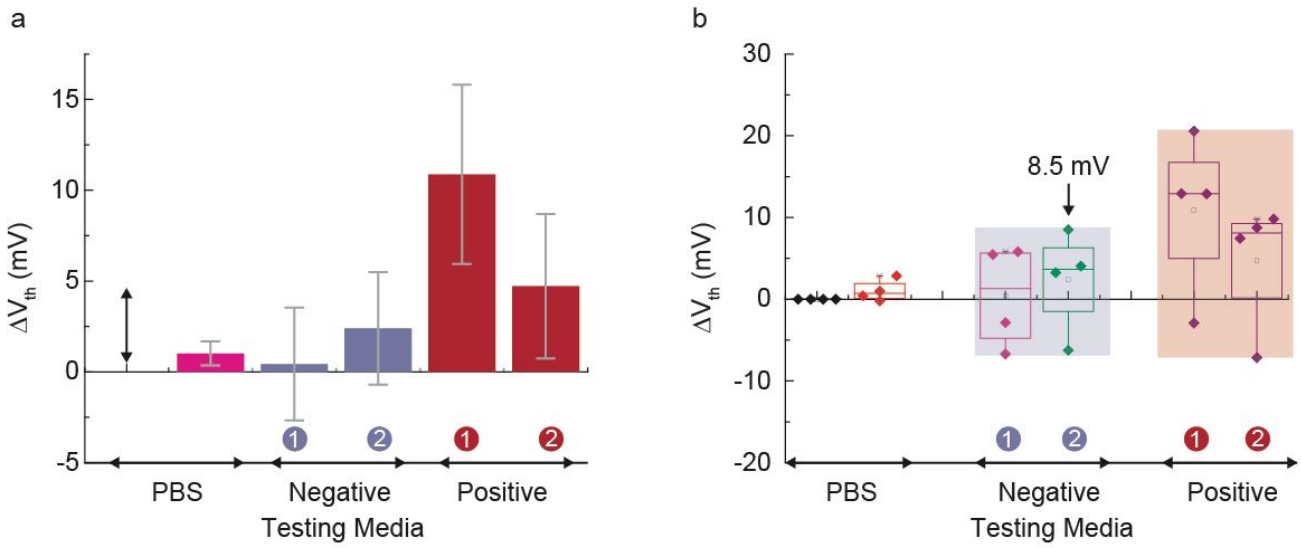

Figure S13. (a) ΔV_{th} levels of rGO with NAb probes vs. nasopharyngeal swab samples diluted in 1 ml PBS that have previously been tested as positive or negative; each sample was measured with 4 different rGO devices. The testing protocol is identical to that of Figure 3a except for a volume of 0.05X PBS for dilutions of nasal swab samples. (b) Distributions of raw data of ΔV_{th} in Figure S13a. A maximum positive ΔV_{th} from samples tested negative is 8.5 mV, which is defined as a maximum background noise level of this system.